Design and Evaluation of a Portable, Flexible-Use Rocket Thrust Stand

Garett C. Foster[1], Lucas J. Utley[1]
Oklahoma State University, Stillwater, OK, 74078

and

Kurt P. Rouser[2]
Oklahoma State University, Stillwater, OK, 74078

Thrust stands are commonly used to test rocket motors and engines, but often they are designed to test a single motor size or type and lack the ability to be transported easily. Presented here are the design and operation of a mobile thrust stand used for static testing solid and hybrid rocket motors of varying sizes and thrust levels. Applications for the stand, include use for academic purposes, as well as experimental motor research and development. The stand is composed of a linear-bearing rail system that uses interchangeable clamps and a compression load cell. The linear rail system is mounted to a table, which is supported by wheels with brakes. With this simple design, the goals of modularity and mobility are achieved, while producing accurate performance data. A program written in LabVIEW runs both the motor ignition and data acquisition to capture time-resolved thrust data at sample rates up to 25 kHz. This thrust stand has the capability to test motor diameters ranging from 1.5 to 4 inches and thrust levels up to 500 pounds. Preliminary results are presented for the testing of five Aerotech H73J-M solid rocket motors, demonstrating the effectiveness of the thrust stand design. Data collected compares measured performance to the manufacturer provided specifications. The values for total impulse and specific impulse averaged across the five motors differed less than 1% from the manufacturer specifications.

I. Nomenclature

A	=	area
A_e	=	nozzle exit area
F	=	force
F_{avg}	=	average force
$\vec{F}_{ext}$	=	external force
g_c	=	gravitational unit conversion factor
I_{sp}	=	specific impulse
I_t	=	total impulse
$\dot{m}$	=	mass flow rate
$\hat{n}$	=	unit outward normal vector
P_a	=	atmospheric pressure
P_e	=	nozzle exit pressure
S_{dev}	=	standard deviation
t	=	time
t_{burn}	=	motor burn time
$\vec{V}$	=	velocity vector

[1] Undergrad Research Assistant, Mechanical & Aerospace Engineering, 218 Engineering N, AIAA Student Member
[2] Assistant Professor, Mechanical & Aerospace Engineering, 218 Engineering N, AIAA Associate Fellow

V_e = nozzle exit velocity
$\forall$ = volume
ρ = density

II. Introduction

Many rocket thrust stands are limited in their capabilities because they cannot be transported and lack the ability to easily accommodate different test articles. To accommodate new test articles, thrust stands usually require extensive modifications and sometimes complete redesigns which can be time consuming and costly. This lack of versatility inhibits rocket propulsion research and development, especially in university labs and small commercial companies with limited funding. Therefore, there is a need for flexible thrust stands supportive of smaller ventures. Presented here is a versatile thrust stand design that allows for affordable testing of various rocket motor types and sizes.

Mobility and modularity were the key factors in making this thrust stand design versatile. Mobility was accomplished by integrating the thrust stand structure with a rolling table, which allows for easy transportation to different testing sites. Modularity was achieved by designing both the structural and measurement capabilities to handle a wide range of different rocket motor sizes and thrust levels. The thrust stand can secure and accurately measure performance of rocket motors ranging from 1.5 to 4 inches in diameter and 5 to 49 inches in length with few adjustments. These motors can be either commercially purchased or experimentally developed and vary in performance from a few dozen to hundreds of pounds of thrust. Having such a broad range of capabilities, this single thrust stand can support testing for various purposes. At university labs, the thrust stand supports experimental motor development, undergraduate propulsion education, and community outreach. In industry, the thrust stand can support affordable propellant and rocket motor development along with qualification testing for operational use. The objective of this paper is to present the design, rationale and experimental evaluation of this versatile thrust stand. Solid-state composite motors were used for the evaluation in this study.

III. Background and Objectives

Thrust stands are essential to aerospace propulsion research and development because they provide the ability to evaluate propulsion systems prior to regular operational status. The data they yield, primarily time-resolved thrust, can be used in the early-design performance characterization or for refinement in later development of propulsion systems. For a rocket motor to be used in flight, it must be ground tested in the form of a static firing, both for safety and reliability, but also to verify performance. Depending on the mission requirements and rocket type, thrust stands vary in design (e.g., orientation, complexity, etc.).

A. Theory

A rocket propulsion system achieves thrust by ejecting matter at high speeds. The governing equation for a rocket thrust control volume (CV) analysis is shown in Eq. (1), the integral form of the momentum equation based on Newton's Second Law, where g_c is a proportionality constant, t is time, $\vec{V}$ is velocity, ρ is density, $\forall$ is volume, $\hat{n}$ is a unit outward normal vector, A is the control surface (CS) area, and $\vec{F}_{ext}$ represents external forces.

$$\frac{1}{g_c}\frac{\partial}{\partial t}\iiint_{CV}\vec{V}\rho d\forall + \frac{1}{g_c}\iint_{CS}\vec{V}\rho(\vec{V}\cdot\hat{n})dA = \sum\vec{F}_{ext} \tag{1}$$

According to Mattingly [1], the control volume term in Eq. (1) is the "time rate increase of momentum" which refers to time-varying storage of momentum, and the control surface term is the net flux of momentum across the exhaust nozzle exit plane. Rocket motors, in general, do not operate at steady state; however, in this study, the storage term is not measured independently. Additionally, the exhaust flow is assumed to be one-dimensional, such that flow properties are constant across the cross-sectional exit plane. Nozzle erosion due to motor burn is considered to be negligible, such that the nozzle exit area is considered constant. Furthermore, there are no pressure, temperature

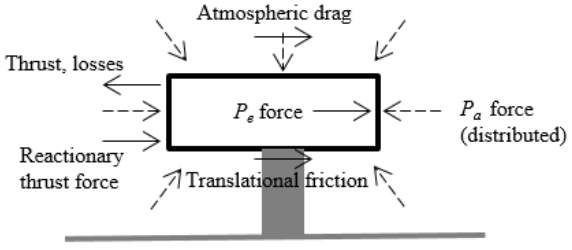

Fig. 1 Thrust stand free body diagram

or velocity measurements made at the nozzle exit plane. The thrust stand designed for this study measures the cumulative external forces acting on the rocket motor. Figure 1 shows a free body diagram of a notional rocket motor thrust stand, including external forces.

The summation force term on the right side of Eq. (1) contains various external forces acting upon a rocket thrust stand. As shown in Fig. 1, these external forces include the reactionary thrust force, atmospheric and exit pressure forces, translational friction, any transmission losses to the load cell, and aerodynamic drag. Except for the reactionary thrust and pressure forces, all other forces are assumed to be negligible compared to the net thrust force, *F*, exerted on the load cell. Equation (2) is reduced to a formulation for axial thrust aligned with primary direction of exhaust velocity.

$$F = \frac{1}{g_c}\frac{\partial}{\partial t}\iiint_{CV} V_e \rho d\forall + \frac{\dot{m}V_e}{g_c} + A_e(P_e - P_a) \tag{2}$$

For example, when exhaust flow and thrust acting in only one "x" direction, the reactionary force, R_x, is measured by the load cell such that $R_x = F$. During a rocket motor firing, Eq. (2) will vary with time throughout the burn duration as V_e, ρ, $\dot{m}$, and P_e are not steady. In neutral-burning motors, these equations may evaluate portions of the time-resolved thrust curve when thrust and chamber conditions change little over a given period, resulting in a level thrust curve. Progressive-burning motors begin with low levels of thrust and increase throughout the burn until the propellant is exhausted. In contrast, regressive burning motors have high initial thrust that decreases over the burn time. Progressive and regressive burns contain time-varying thrust levels and chamber conditions throughout the burn and are not well approximated by Eq. (2).

From time-resolved thrust data, another important figure of merit may be obtained: total impulse, I_t. Thrust integrated over motor burn time, t_{burn}, yields I_t as shown in Eq. (3)

$$I_t = \int_0^{t_{burn}} F dt \tag{3}$$

It is worth noting that rocket motors are often labeled by time-average thrust, F_{avg}. Equation (4) is used to describe motor burn performance in terms of F_{avg} as produced throughout the rocket motor burn time.

$$I_t = F_{avg} t_{burn} \tag{4}$$

Specific impulse, I_{sp}, is another performance figure of merit, representing the impulse per unit weight of propellant as shown in Eq. (5) from Sutton [2]. Specific impulse describes the fuel efficiency of a rocket motor and its associated propellant. For example, a high-performance rocket motor, having a high I_{sp}, effectively converts an energy-dense propellant into thrust.

$$I_{sp} = \frac{\int_0^{t_{burn}} F dt}{g \int_0^{t_{burn}} \dot{m} dt} \tag{5}$$

The above equations and figures of merit describe the parameters involved in evaluating rocket motor performance. Total impulse describes how powerful a motor is; whereas, specific impulse describes how efficient a motor is. Peak thrust, average thrust, and burn duration are useful parameters in characterizing the performance of an experimental motor or validating the performance of a commercial motor.

B. Thrust Stand Architecture

Thrust stands for solid rocket motors have three key components: thrust stand structure, a method for translation/deflection, and a load cell. As prescribed by Runyan et al [3] the design of a thrust stand must consider several factors such as specifying the test article type, size and configuration, force/accuracy requirements, and test facility constraints. Each of these factors influenced the selection and design of the three thrust stand components mentioned above.

1. Thrust Stand Structure and Orientation

Thrust stand orientations vary depending on the type of propulsion system to be analyzed. Overall, thrust stands can be categorized into either vertical or horizontal referring to the orientation of the test article. Simplified drawings and real world examples of each are shown in Fig. 2

Liquid propellant engines are typically tested vertically with the nozzle and exhaust directed downwards because the fuel and oxidizer tanks must be drained from the bottom as would be the case in flight under acceleration forces. Solid and hybrid motors can also be tested vertically similar to liquids but are more commonly found horizontally. With the test article(s) for the stand designed in this study being primarily solid rocket motors, a horizontal orientation was initially selected for the thrust stand structure. This decision is supported by Runyan et al [3] who point out that with solid rocket motors, the changing motor weight does not influence the thrust produced. The benefit of this orientation is that it allows for a less complex and more compact thrust stand structure that can be easily and affordably reconfigured, especially when considering facility constraints.

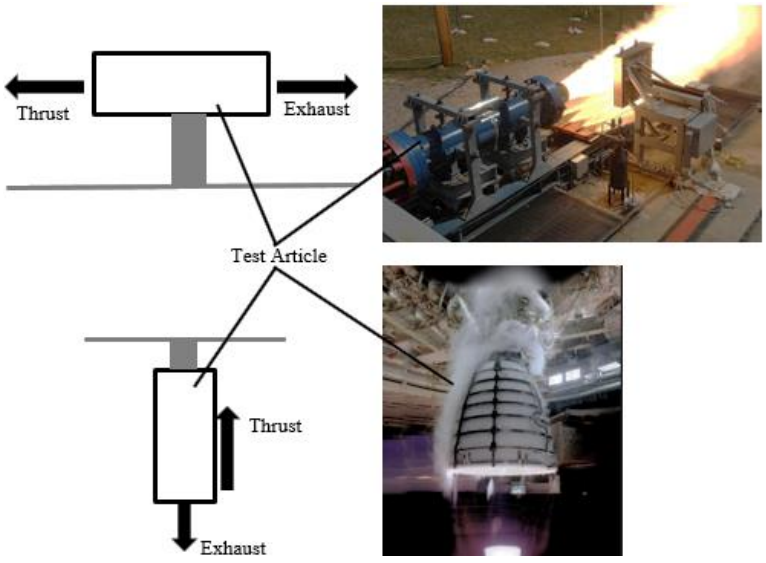

Fig. 2 Horizontal orientation (top left) & example (top right)[4], Vertical orientation (bottom left) & example (bottom right)[4]

Another structural suggestion from Runyan et al [3] is that that a thrust stand design should incorporate adaptability in order to meet a variety of test article requirements. This design element of adaptability was central to the design of the thrust stand presented here but is not a common element found in most thrust stands. Figure 3 to the right demonstrates the size range of different rocket motors to be used as test articles on the stand presented here.

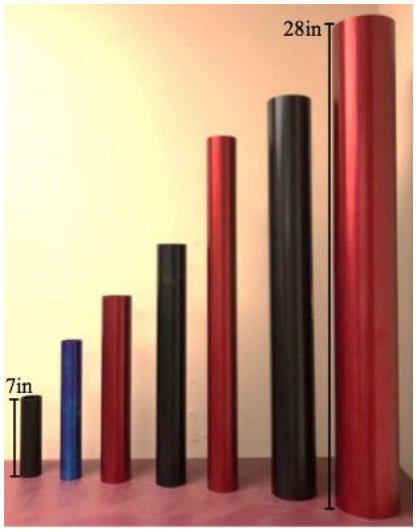

Fig. 3 Casing size range example

2. Load Transfer Method

Most thrust stand designs fall into one of two categories for their load transfer method. The first, and more common, is on-axis measurement where the load cell is on the axis of the thrust force vector produced by the test article. The second is off-axis measurement where the load cell is away from the thrust force vector; this category is more common in air-breathing propulsion thrust stands (Runyan et al [3]). In this case, the load cell may still be parallel to the thrust vector or orthogonal with a moment arm.

Simple schematics of each type of load transfer method are shown below. Whether on- or off-axis, thrust stands most often use some form of linear bearing to allow for the translation of thrust force, except in the moment-arm design where a rotational bearing may be used.

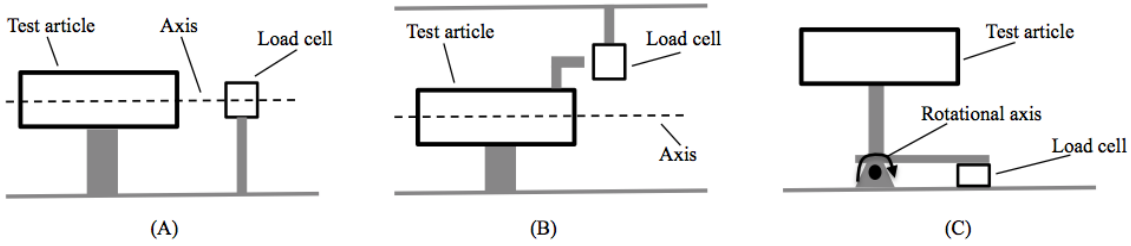

Fig. 4 Load transfer method (A) On-Axis, (B) Off-Axis, (C) Moment-Arm

With the considerations of test article, and in an effort to avoid complex calibrations, an on-axis load transfer method was selected with use of linear bearings. A similar approach was used by Mondragon and Hubbard [5] who designed a thrust stand that utilizes two rails and an on-axis load cell to measure dynamic thrust stand properties. The design here is focused solely on thrust and developing a thrust stand that can accommodate a variety of motor sizes and thrust levels.

3. Load Cell

Central to the thrust stand is the load cell which allows for thrust measurement. Load cells may be designed in-house or commercially purchased. The purpose of the load cell is to convert mechanical force input into an electrical signal output, typically voltage. By use of a calibration curve, the electrical signal can be converted back to the corresponding force input. Considering the objectives of this design, which are focused more on the overall thrust stand structure and its uses, it was decided to purchase an off-the-shelf compression load cell with an adequate load range. This same decision was made in the thrust stand designed by Thomas et al [6], who used an Omega Engineering commercial load cell. The off-the-shelf option, while sometimes more expensive, helps to increase the accuracy of measurements and provides an ability for compact and custom load cells.

C. Objectives

The objective of this study is to present the detailed design, rationale, and evaluation of a versatile rocket thrust stand. The evaluation is accomplished by a series of H73J-M rocket motor tests. The figures of merit for the evaluation include time-averaged and time-resolved thrust, as well as total and specific impulse. A comparison is made of performance between motors and against the motor manufacturer specifications.

IV. Design

To begin design, a series of more specific criteria was made related to the thrust stand structure and test articles. With a budget of approximately $2000, it was decided to keep any custom fabrication to a minimum and build the structure largely with off-the-shelf parts. A range of motor diameters was defined to include 1.5, 2.1, 3.0, and 4.0 inch motors, which are standard casing sizes in high power rocketry. These diameters include motors from H-class (35 lbf·s - 72 lbf·s) to M-class (1151 lbf·s - 2302 lbf·s) total impulse and range in length from 5 to 49 inches. For thrust, a max of 500 pounds was set and used to size the load cell.

A. Structural Design

Given the parameters of accommodating motor diameters, lengths, and thrust ranges, multiple design iterations were performed. Common design elements between each iteration were the use of 1.5-inch t-slotted aluminum framing and linear bearings. The final design is shown below.

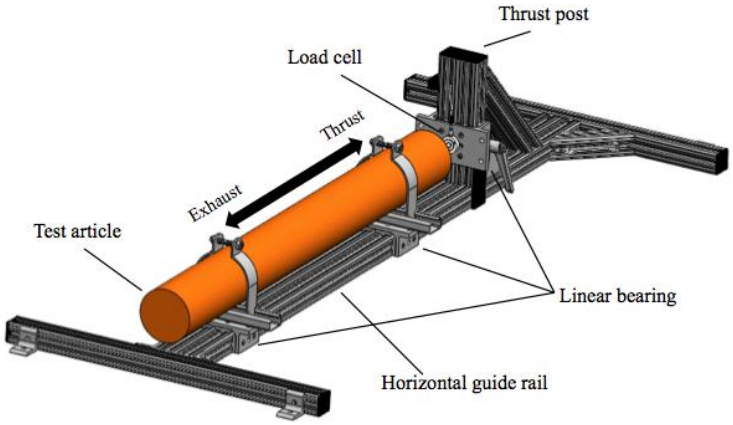

Fig. 5 Thrust stand structure with 4x40 inch motor

The primary features of this design are a horizontal 1.5x3.0 inch T-Slotted guide rail, a 1.5x3.0 inch T-Slotted vertical thrust post and three linear bearings. The two horizontal linear bearings translate along the guide rail and can be spaced apart at different distances to accommodate different motor lengths. The vertical thrust post, which braces

against thrust force loads, is supported by a diagonal brace and corner brace opposite the thrust loads. This thrust post can translate along the guide rail by loosening the two braces. Moving the thrust post allows for different motor lengths to be positioned with the nozzle over the end of the thrust stand. The thrust post also guides a linear bearing vertically which is used to adjust the load cell height.

The load cell, which measures thrust force, is mounted to the thrust post linear bearing using an adapter plate. This adapter plate, shown to the right in Fig. 6, is one of few custom fabricated parts on the thrust stand. The plate was used instead of mounting the load cell directly to the linear bearing to allow for flexibility in the case that the load cell ever need changed out for another.

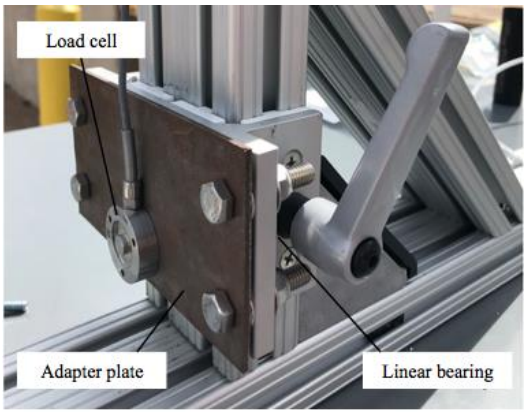

Fig. 6 Vertical linear bearing and load cell

Most of the elements of this thrust stand were designed with modularity in mind. One of those elements, as aforementioned is the linear bearings. The other elements are the strut channel and routing clamps used to secure motors to the linear bearings. As shown in Fig. 7 below, a single piece of aluminum strut channel was attached to each horizontal linear bearing. Different sizes of standard routing clamps designed for strut channel can then be used to secure a range of motor sizes to the thrust stand. Figure 7 demonstrates the use of different routing clamp sizes along with the different degrees of freedom that this thrust stand has.

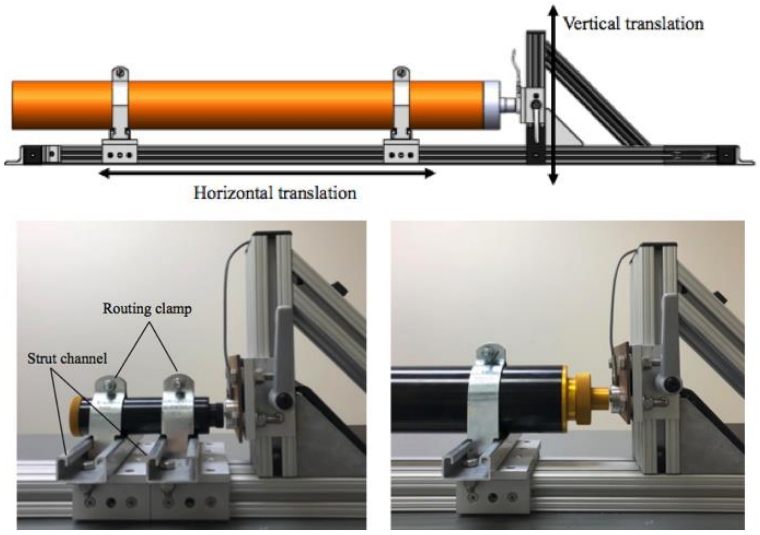

Fig. 7 Thrust stand side profile (top), 1.5-inch diameter motor (bottom left), 3-inch diameter motor (bottom right)

The final element of the structural design of this thrust stand was attaching it to a large steel table. The table with its four locking wheels allows for the thrust stand to be mobile and provides a space for all data acquisition and measurement components. Securing the T-Slotted aluminum structure to the steel table was done with eight brackets using 5/16” nuts and bolts. The completed thrust stand is shown in Fig.8.

In Fig.8 the thrust stand is configured for a small motor. Therefore, the thrust post is left of center. The thrust stand lower shelf is used for storage of tools, extension cords and weights all necessary for rocket motor testing. The instrument cluster is attached to the table on the right side.

Fig. 8 Thrust stand

B. Measurement Systems Design

The measurement system for this thrust stand consists of multiple components which are grouped in three categories; Control, Ignition and Measurement. The system power and signal paths are shown in the figure below.

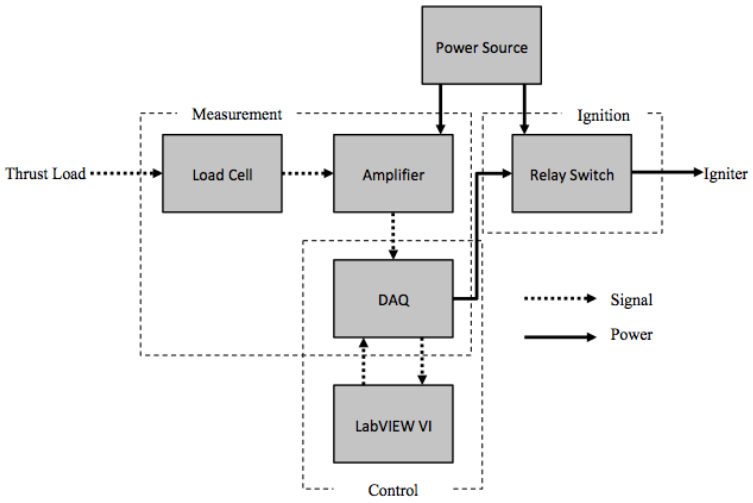

Fig. 9 Measurement system power and signal paths

The entirety of the measurement system is controlled by a custom LabVIEW VI program that was developed for the stand. This VI, in connection with the Data Acquisition Card (DAQ) is able to initiate motor firings and collect time-resolved thrust data from the load cell. For the DAQ, a simple National Instruments USB-6009 Multifunction Card was used. The DAQ Card has both input and output signals that communicate between the VI, amplifier and relay switch.

Powering the load cell/amplifier is a National Instruments PS-15 Power Supply. This power supply is used to provide clean power to the Futek LLB400 Load Button Load Cell, Futek IAA100 Voltage Amplifier, and a relay switch that controls rocket motor ignition. The instrument rail containing the power supply, load cell amplifier, ignition relay switch and DAQ Card is displayed in Fig. 10 to the right.

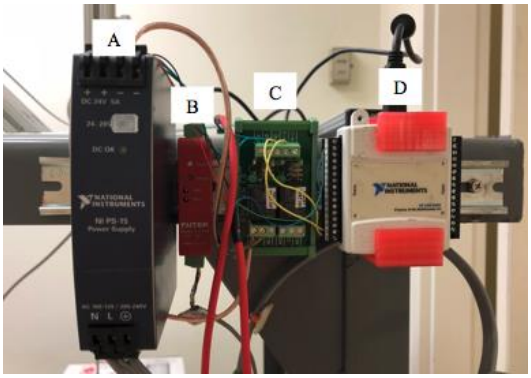

Fig. 10 Instrument rail: (A) Power supply, (B) Amplifier, (C) Relay switch, (D) DAQ

C. Preload Design

As a final addition to the thrust stand design, a preload system was incorporated. Preloading the load cell is intended to aid in calibration of the system and to improve data quality. The preload design was done using cable-pulley system with deadweight hanging under the thrust stand table top surface. An adapter attaches to the rocket motor and transfers the hanging weight to the load cell. Figure 11 below highlights the preload design.

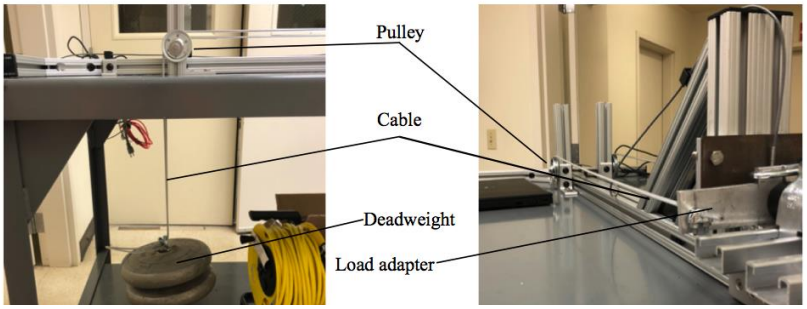

Fig. 11 Thrust stand preload design

V. Experimental Setup and Procedures

Thrust stand operation and rocket motor testing was conducted at the Oklahoma State University Richmond Hill Research Center. The thrust stand was flush against a concrete wall of a loading dock with the wheels locked to limit any movement by the table. For testing, the Aerotech H73J-M motor with its respective 38/240 standard casing was used with a plugged forward closure. The closure contains a flat surface that rests against the load cell. Before each motor firing, adjustments were made to the thrust post and linear bearing positions to ensure the motor exhaust would not impinge on the thrust stand structure. The thrust stand configuration for these tests can be observed in Fig. 8. Tests were conducted using a sample rate of 100 Hz.

Once the test article was secured and igniter placed in the motor, it was connected to the instrument cluster and the instrumentation powered on. The LabVIEW VI controlled the ignition and data collection commands and the motor fired when ready. Following the test, the data was analyzed, and the stand recycled for the next test.

A. Procedures

The thrust stand is housed and stored in the Propulsion Laboratory of the Richmond Hill Research Center. Motors are assembled and prepared for firing but not yet secured to the stand. The stand's mobility allows it to be moved through the building to the loading dock and pushed against a concrete wall. The loading dock offers a clear path downrange of the motor exhaust and electricity for operating the stand.

When the stand is securely in place, the thrust post is moved into position then secured. Next, the prepared motor is attached to the stand by means of the linear bearings and adjustable routing clamps. The bearings are moved into position to support each end of the motor, and the clamps lock the motor into place atop the bearings. The preload support is removed and suspends the preload weight prior to the test.

The motor's igniter is connected via clips and inserted into the motor. At this point, the hardware is ready for the firing. Power is given to the instrument cluster and a "click" is audible as the cluster's power supply turns on.

The remaining actions take place remotely from the LabVIEW VI shown in Fig. 12. Proceeding through the software interface, there are sequential steps in the program that ensure motor firing takes place when all systems are ready. At the "FIRE" command, the system begins collecting thrust values from the load cell at the selected frequency. The power supply trips the electronic relay to send current through the igniter. The igniter burns which brings the motor up to pressure. Most motor burns last 1-3 seconds, but a built-in delay charge burns for another 6-14 seconds. This charge is for the coast phase, had the motor been used in flight. Following motor burnout, the VI is ended by the operator, and data acquisition stops at that time. Power is disconnected. Once the delay charge burns out, the stand may be approached, and the hot motor removed then the stand refitted with a new motor. The burned igniter is discarded and a new one used with a new motor.

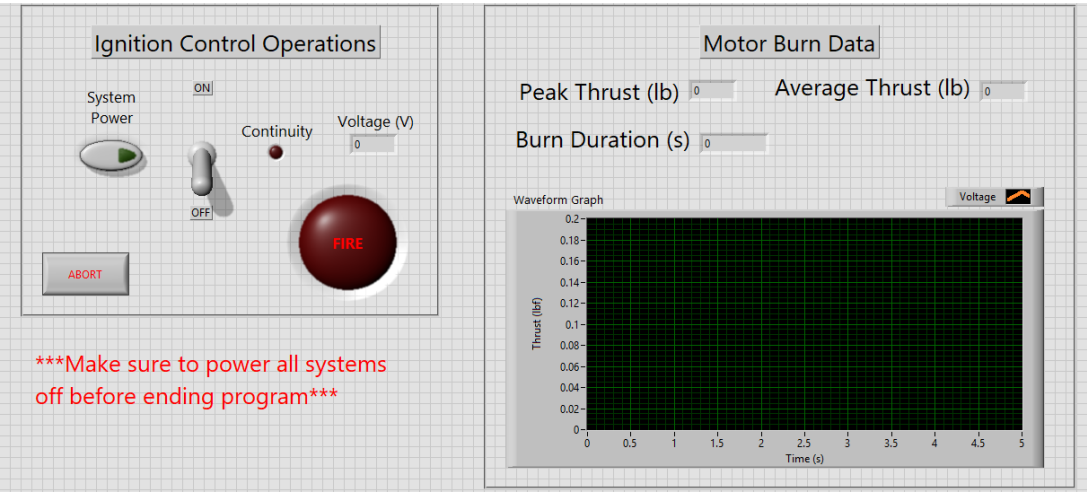

Fig. 12 LabVIEW control panel for rocket motor testing

VI. Results

After the five H73J-M motor tests, each motor data file was reduced by subtracting the preload weight from the thrust and trimming the time to the duration of motor firing. From the reduced data files, peak thrust and burn time were found, then average thrust was calculated for each of the five motors. Those values were then used, along with the manufacture given motor propellant weight to calculate total impulse and specific impulse. It was assumed that all propellant was burned in each motor firing. Table 1 below shows the performance values for each motor as well as the average values and standard deviation across the five motors. Furthermore, the table shows comparisons of the average values to the given manufacturer data.

Motor	Peak Thrust (lbf)	Average Thrust (lbf)	Burn Time (s)	Total Impulse (lbf-s)	Specific Impulse (s)
1	17.73	10.45	3.89	40.66	147.86
2	21.82	10.99	3.72	40.88	148.67
3	18.49	12.45	3.39	42.19	153.45
4	22.22	12.00	3.49	41.88	152.30
5	22.16	10.73	3.57	38.32	139.35
Average	20.48	11.32	3.61	40.79	148.33
Standard Deviation	9.6%	6.8%	4.9%	3.3%	3.3%
Manufacturer	15.68	16.41	3.5	40.47	147.16
% Difference Manufacturer to Average	-30.6%	31.0%	-3.2%	-0.8%	-0.8%

Table 1 Aerotech H73J-M experimental test and manufacturer data

Comparing the average burn time across the five motors to the manufacture specified burn time gives a percent difference that is low. This value could be further improved by additional testing and more closely tracking motor ignition and burn time using other methods such as video. Both total impulse and specific impulse have percent differences under 1%, a promising result in evaluating the thrust stand. These results show that the stand is measuring the same power and fuel efficiency from the motors as they are intended to produce. Average thrust for the tested motors was much lower than the manufacturer's value. The manufacturer's average thrust comes from the motor designation (73 Newtons average thrust), but does not match with the thrust data provided by the manufacturer. This inconsistency might mean the manufacture uses a different method for finding average thrust than used here. The peak thrust also had a large percent difference, with the tested motors having much higher values than the manufacturer. Peak thrust however, is better evaluated using time-resolved data.

Figure 13 to the right shows the time-resolved thrust curves for each of the five motor tests. It is clear from these plots that the unsteady assumption previously made is valid. Looking at

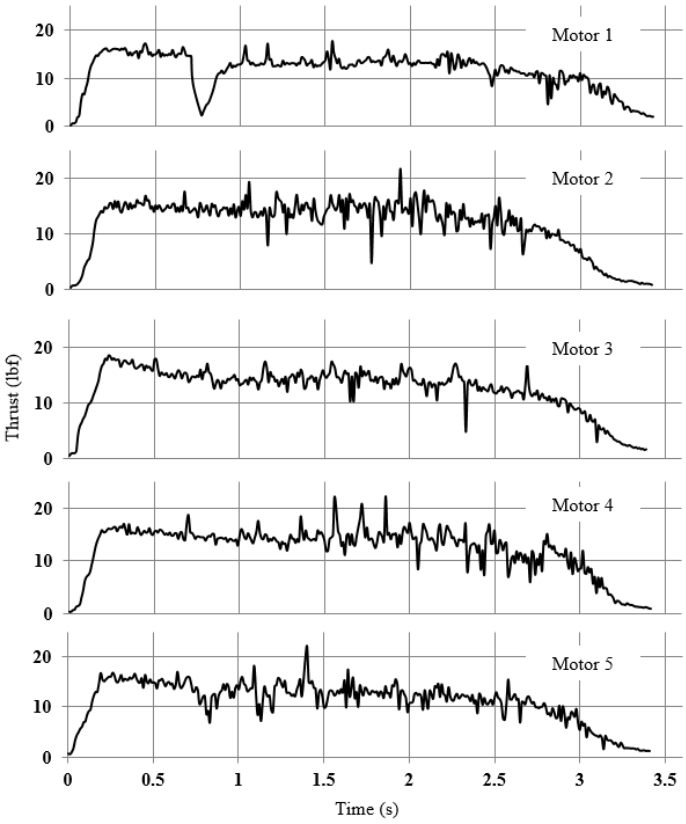

Fig. 13 Thrust curves for 5 tested H73J-M motors

the peak values, it can be noted that many of the peaks occur well after the motor ignition. The peaks occur when the motor would typically be more neutral burning. This could be due to the thrust stand being more sensitive to thrust variations. During the motor firings, loud "pops" were audible and observed in the smoke plume which could also explain the various peaks. Motor 1 has a large aberration around the 0.75 second point, this could be attributed to an issue with the thrust stand such as a linear bearing sticking or to inconsistencies in the motor propellant grain such as an air pocket (not uncommon in propellant grains).

Figure 14 below shows an ensemble average plot with thrust averaged across each of the 5 motors over a common time span. Also included are plots of standard deviation across the 5 motors both added and subtracted from the average thrust. In this plot, the aberration noticed in motor 1 clearly has an influence at the same 0.75 second point.

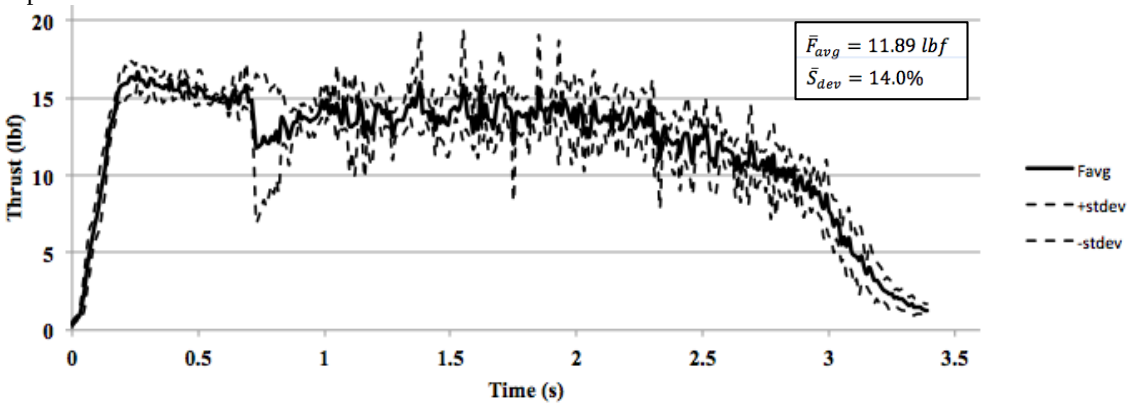

Fig. 14 Motors 1-5 ensemble average thrust plot

The ensemble plot above can be used to address uncertainty. Due to the small sample size of only five motors, methods such as the Kline McClintock method to calculate overall uncertainty were not used. The maximum error of the load cell and amplifier is 0.086 % readout as specified by the Futek calibration. Compared to the standard deviation, this instrumentation uncertainty is negligible. The average standard deviation for the ensemble plot above is 14.0% of the average thrust. However, if motor 1 is removed due to its inconsistency, the standard deviation improves to 12.3% of the average thrust. Noting this trend, motor 1 was removed from the data set before further evaluating the time-resolved performance.

Figure 15 below is the ensemble average plot using motors 2-5 with the addition of the manufacturers given thrust curve for the H73J-M motor shown as the thick dashed line. Standard deviation was not plotted but the value as a percent of average thrust is shown on the plot. It was not explicitly stated by the manufacturer, but the given data corresponded to a sample rate of just above 3 Hz. The manufacturers data may be from a moving average and not directly from measurements.

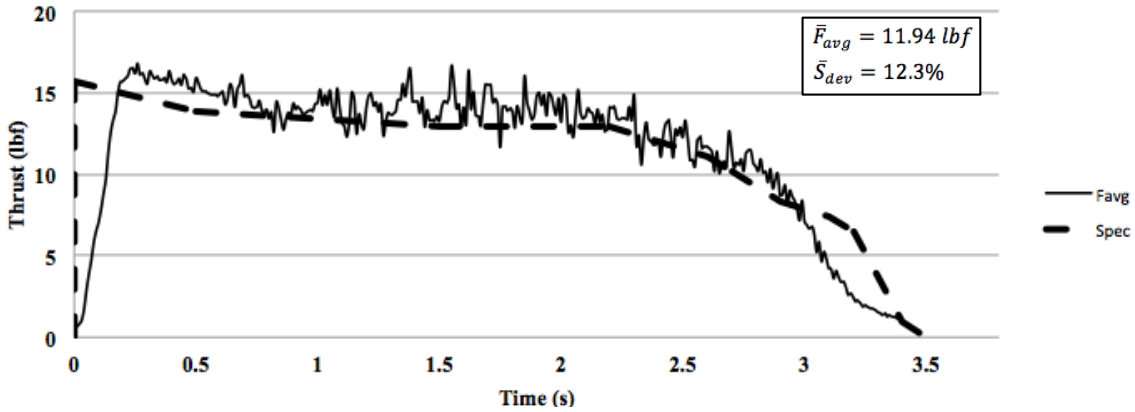

Fig. 15 Motors 2-5 ensemble average thrust plot

With motor 1 removed from the ensemble average, a more consistent thrust curve is produced. The trend of the ensemble average closely resembles that of the manufacturers thrust curve. As mentioned above, the manufacturers specified average thrust of 16.41 pounds did not match with the provided data. This can be visualized in Fig. 15

where the manufacturers curve is below the four motor ensemble average. The consistent trend between the averaged data and the manufacturers data along with the percent differences for burn time, total impulse, and specific impulse shown in Table 1 provides external validation for the thrust stand design. Figure 16 below shows one of the H73J-M motor tests.

Fig. 16 Aerotech H73J-M motor test firing

VII. Summary and Recommendations

The thrust stand design, rationale and evaluation presented in this paper demonstrate a versatile thrust stand with the capability to support testing by various groups. The evaluation, which showed the thrust stand to be effective at measuring time-resolved thrust, is representative of the type of university and industry testing that the stand could be used for. The results were not able to fully validate the thrust stand due to inconsistencies in rocket motor tests and with the manufacturer provided performance data. It is recommended that further evaluation of the thrust stand take place.

Future testing should include a larger sample size of rocket motors to better address uncertainty. Future testing should also be done with varying sizes and thrust levels of rocket motors to evaluate the stand with different configurations (i.e., moving thrust post or using different motor clamps). It is also recommended that further analysis take place to evaluate the structural limitations of the thrust stand.

Acknowledgments

Garett Foster and Lucas Utley would like to thank Tyler Zimbelman, Elon Musk, Matt Durkee, Drew Bellcock and Nick Lucido.

References

[1] Mattingly, J.D., and Boyer K.M., *Elements of Propulsion: Gas Turbines and Rockets*, 2nd ed., AIAA Education Series, AIAA, New York, 2016

[2] Sutton, G.P., Biblarz, O., *Rocket Propulsion Elements*, 8th ed., John Wiley & Sons, Inc., Hoboken, NJ, 2010, pp. 28-29.

[3] Runyan, R.B., Rynd, J.P., Jr., and Seely, J.F., "Thrust Stand Design Principles," AIAA-92-3976, 1992.

[4] www.nasa.gov

[5] Mondragon, J.M., and Hubbard, J.E., Jr., "Design, Build, and Test of a Test Thrust Stand," AIAA 2017-0104, 2017.

[6] Thomas, J.C., Stahl, J.M., Morrow, G.R., and Petersen, E.L., "Design and Characterization of a Lab-Scale Hybrid Rocket Test Stand," AIAA/SAE/ASEE Joint Propulsion Conference 2016., Salt Lake City, UT, 2016.